A Flow-informed Strategy for Ballistic Capture Orbit Generation

M. Manzi · F. Topputo

Abstract Ballistic capture is a phenomenon by which a spacecraft approaches its target body, and performs a number of revolutions around it, without requiring manoeuvres in between. Capture orbits are characterized by specific dynamics, defining regions that guide transport phenomena. Because of the limitations associated with existing approaches, the development of heuristics informed by Lagrangian Coherent Structures appears desirable. In fact, such structures identify transport barriers in dynamical systems, separating regions with qualitatively different dynamics.

In this work, different flow-informed approaches are presented, and their relations with ballistic capture are discussed. A new heuristic, the time-varying strainline, is introduced. This new tool is applied to compute ballistic capture orbits around Mars. Different degrees of model fidelity have been investigated, mainly in order to test the robustness of the proposed technique with respect to different features of the underlying dynamical model. We show that time-varying strainlines are useful in identifying ballistic capture orbits.

Keywords Ballistic capture, Weak Stability Boundary, Low-energy Transfers, Lagrangian Coherent Structures, Lyapunov Exponents, Time-varying Strainlines

M. Manzi (✉)
Department of Mechanical and Aerospace Engineering, University of Strathclyde,
75 Montrose Street, Glasgow G1 1XJ, United Kingdom
E-mail: matteo.manzi@strath.ac.uk

F. Topputo
Department of Aerospace Science and Technology, Politecnico di Milano,
Via La Masa 34, 20156 Milan, Italy
E-mail: francesco.topputo@polimi.it

This is a peer-reviewed, accepted author manuscript of the following article: Manzi, M., & Topputo, F. (2021). A flow-informed strategy for ballistic capture orbit generation. Celestial Mechanics and Dynamical Astronomy, 133(11-12), [54]. https://doi.org/10.1007/s10569-021-10048-2

1 Introduction

Mission design is a trade-off between model accuracy and design feasibility. With the development of tools to tackle complex systems, their understanding is expanded and new solutions are revealed. The space community is therefore focusing on the exploitation of dynamical nuances of the solar system: low-energy transfers are a new design ingredient made available by such approach.

A family of low-energy transfer trajectories is given by the ones making use of ballistic capture: these are natural orbits characterized by a small excess velocity upon arrival to a target body (Belbruno and Miller, 1993). Ballistic capture orbits are interesting from a space mission design point of view. In fact, making use of more traditional approaches, some designs are excluded in an early stage; moreover, in order to deal with the possibility of single point failures, strict robustness requirements have to be satisfied (Schoenmaekers, 2004; Jehn et al., 2004). Ballistic capture orbits are attractive also because of their wider launch windows, since the alignment between the Earth and the target body is not necessary (Topputo and Belbruno, 2009). The use of low-energy transfers has been recently proposed for a number of space missions (Koon et al., 2001a; Topputo and Belbruno, 2015; Mazanek et al., 2013; Cox et al., 2019).

Ballistic capture trajectories make use of the chaotic nature and, in general, of the nuances of the dynamical system causing the motion (Short et al., 2015). In order to make their implementation feasible, the introduction of flow-informed strategies appears desirable. Developed in works focused on hyperbolic Lagrangian Coherent Structures (LCSs), this research project builds on the Finite-Time Lyapunov Exponent (FTLE) and the Finite-Iteration Lyapunov Exponent (FILE) scalar fields (Haller, 2010; Farazmand and Haller, 2012; Gawlik et al., 2009). Such structures are an attempt to generalize the concept of invariant manifolds, separating regions of the phase space associated to qualitatively different behaviours: they are defined in non-autonomous systems and, when applied to autonomous ones, they coincide with invariant manifolds (Teramoto et al. (2013)).

The objective of this work, expressed in high level terms, deals with further developing the theoretical underpinning of low-energy transfer orbits, by making use of LCSs in time-dependent dynamical systems. As a secondary goal, the *secondary theoretical comparison* between traditional methods related to the ballistic capture literature and the ones coming from the LCS field of research, makes it possible to contribute building an encompassing theory.

A number of reasons justify the use of LCS in ballistic capture trajectory design, together with the development of related tools and heuristics: the application of analytical, differential instruments leads to high-accuracy results; applicability in arbitrary subsets of the phase space is desirable, in order to gain insights into the phenomenon. The potential reduction of computational cost can increase the applicability of the technique for the Guidance, Navigation, and Control (GNC) system of autonomous missions; at the same time, the proposed flow-informed approach can be superimposed onto models of different fidelities, making it suitable for different phases of the trajectory design process.

This is done building from a number of existing heuristics and flow-informed approaches; in particular, the strain tensor associated to astrodynamics dynamical systems is analyzed in order to compute ballistic capture orbits, via the computation of time-varying stroboscopic strainlines, here introduced. In this way the phase space can be divided into dynamically distinct regions.

The paper is structured as follows. Section 2 presents the various reference frames and the equations of motion used in this work; the variational equations, leading to the Cauchy–Green (CG) Strain Tensor, are also discussed here. Section 3 focuses on the ballistic capture phenomenon, defining the *Capture Set* and the *Weak Stability Boundary* (WSB). Section 4 leads from existing scalar fields to the definition of *Time-varying Strainlines*, the core idea of this work. Section 5 presents the results comparing traditional algorithms with the given flow-informed approach. The geometry of the resulting trajectories will be given and discussed; also, a flow-informed strategy, applicable to construct ballistic capture trajectories, will be outlined. Section 6 contains the conclusions, underlining areas in which future developments appear desirable.

2 Background

2.1 Reference Frames and Equations of Motion

2.1.1 Reference Frames

In order to implement a real ephemerides models, making use of the SPICE Toolkit[1], the *Earth Mean Equator and Equinox of J2000* (EME2000) reference frame is introduced (Luo et al., 2014). This is an Earth centered inertial reference frame, where the +x-axis (x_e) points at the mean equinox at J2000, the +z-axis (z_e) points at the celestial North Pole and the +y-axis (y_e) completes the right-handed reference frame (Wakker, 2015).

In literature, the ballistic capture phenomenon has mainly been studied with respect to reference frames related to the orbit of the target body; in the Radial-Tangent-Normal frame at epoch t_0 (RTN@t_0, for brevity), centred at the target body, the z-axis (z_r) is perpendicular to the plane of the Sun orbit, the x-axis (x_r) is aligned with the Sun-planet line, pointing from the Sun to the planet and the y-axis (y_r) completes the dextral orthonormal triad. The transformation from the RTN@t_0 to the EME2000 can be found in Luo and Topputo (2015).

An additional reference frame, the *Roto-pulsating reference frame*, introduced in Dei Tos and Topputo (2017), has been used to represent the results given in Section 5: this allows to compare results from models of different fidelities, and better understand the effect of specific perturbations.

2.1.2 Equations of Motion

The proposed flow-informed technique can be superimposed onto models of different fidelities: because of this, a restricted n-body problem, with the addition of

[1] `https://naif.jpl.nasa.gov/naif/toolkit.html` - last visited: 11-05-2021

Solar Radiation Pressure (SRP) and Non-Spherical Gravity (NSG), will be used to formulate the equations of motion.

Considering a system of n bodies, $n-1$ of which called primaries, it is interesting to study the motion of a particle of negligible mass with respect to them. Following Luo and Topputo (2015), in order to underline the hierarchy of influence of the bodies on the motion of the particle, the motion is governed by:

$$\ddot{\mathbf{r}} + \frac{\mu_t}{r^3}\mathbf{r} + \mu_s \left(\frac{\mathbf{r}_s}{r_s^3} + \frac{\mathbf{r}-\mathbf{r}_s}{||\mathbf{r}-\mathbf{r}_s||^3} \right) = -\sum_{i \in \mathbb{Q}} \mu_i \left(\frac{\mathbf{r}_i}{r_i^3} + \frac{\mathbf{r}-\mathbf{r}_i}{||\mathbf{r}-\mathbf{r}_i||^3} \right) \tag{1}$$

In Equation (1), $\mathbf{r}$ identifies the position of the spacecraft with respect to the origin of the reference frame, in which the target body is located; r is the magnitude of that vector. μ_t is the gravitational parameter of the target body and μ_i the one of body i; $\mathbf{r}_i$ is the position vector of body i and r_i is its magnitude. Finally, $\mathbb{Q}$ is the set of $n-3$ perturbing bodies, Sun excluded.

When SRP and the NSG of the target body are taken into account (Aguiar and Topputo, 2018), the dynamics is governed by:

$$\ddot{\mathbf{r}} + \frac{\mu_t}{r^3}\mathbf{r} + \mu_s \left(\frac{\mathbf{r}_s}{r_s^3} + \frac{\mathbf{r}-\mathbf{r}_s}{||\mathbf{r}-\mathbf{r}_s||^3} \right) + Q_{f\to i}(t)\nabla U_{NSG} = \\ = \mathbf{f}_{SRP} - \sum_{i \in \mathbb{Q}} \mu_i \left(\frac{\mathbf{r}_i}{r_i^3} + \frac{\mathbf{r}-\mathbf{r}_i}{||\mathbf{r}-\mathbf{r}_i||^3} \right) \tag{2}$$

The effect of (cannonball) SRP is modelled using (Wakker, 2015):

$$\mathbf{f}_{SRP} = \frac{C_R L_S}{4\pi c} \frac{A}{m} \frac{\mathbf{r}-\mathbf{r}_s}{||\mathbf{r}-\mathbf{r}_s||^3} \tag{3}$$

where L_S is the luminosity of the Sun, c is the speed of light, C_r is the reflectivity of the spacecraft and A and m are its effective area and mass, both assumed constants; $\mathbf{r}$ and $\mathbf{r}_s$ are the position vectors of the spacecraft and of the Sun, respectively.

U_{NSG} is an approximation of the gravitational potential function of the target body (Wakker, 2015), given by:

$$U_{NSG} = \frac{\mu}{r}\left[\sum_{n=2}^{\infty} J_n \left(\frac{R}{r} \right)^n P_n(\sin\phi) + \right. \\ \left. + \sum_{n=2}^{\infty} \sum_{m=1}^{n} J_{n,m} \left(\frac{R}{r} \right)^n P_{n,m}(\sin\phi)\cos m(\Lambda - \Lambda_{n,m}) \right] \tag{4}$$

In Equation (4), $P_n()$ and $P_{n,m}()$ are Legendre polynomials and associated Legendre functions of the first kind, R is the reference radius, r the distance from the body center of mass and μ its standard gravitational parameter; ϕ is the geocentric latitude, Λ is the geographic longitude. These spherical coordinates are relative to a target-fixed reference frame, centred at the barycenter.

Finally, in Equation (2), $Q_{f\to i}$ is the rotation matrix relating the planet-fixed reference frame, in which U_{NSG} is defined, and the pseudo-inertial reference frame, in which the equations of motion are written.

2.2 Variational Equations

Independently of the active terms in Equation (2), once the reference frame is given, the motion of the massless body can be described by the differential equation associated to the state of the system, which allows one to reduce the order of the differential equation at the expenses of doubling the dimensionality of the problem:

$$\begin{cases} \dot{\mathbf{x}}(t) &= \mathbf{f}(\mathbf{x}(t), t) \\ \mathbf{x}(t_0) &= \mathbf{x}_0 \end{cases} \tag{5}$$

with $\mathbf{x}(t) \in \Omega \subseteq \mathbb{R}^6$. As usual, the first order differential equation (the *velocity map*) can be obtained at the expenses of doubling the number of independent variables of the system (Meiss, 2007). Because of the nature of the (perturbed) n-body problem presented above, there is a direct dependence with respect to time in the velocity: the system is non-autonomous.

Using such formalism, the *State Transition Matrix* (STM) is defined by:

$$\mathbf{\Phi} := \mathbf{\Phi}(t; t_0, \mathbf{x}_0) = D_{\mathbf{x}_0}\mathbf{x}(t; t_0, \mathbf{x}_0) \tag{6}$$

and its propagation can be performed by means of:

$$\begin{cases} \dot{\mathbf{\Phi}} = D_{\mathbf{x}}\mathbf{f}(\mathbf{x}, t)\mathbf{\Phi} \\ \mathbf{\Phi}(t_0; t_0, \mathbf{x}_0) = \mathbf{I}_n \end{cases} \tag{7}$$

where $D_{\mathbf{x}}\mathbf{f}(\mathbf{x}, t)$ is the Jacobian of the velocity field and $\mathbf{I}_n$ is the identity matrix of size n; the derivation of Equation (7) is given, among others, in Milani and Gronchi (2004). The joint system, characterized by $n + n^2$ independent variables, defines the *Variational equations*, allowing to propagate the STM of the dynamical system.

2.2.1 Cauchy–Green Strain Tensor

The (Finite-time) CG Strain Tensor can now be introduced:

$$\mathit{\Delta}(T, \mathbf{x}_0, t_0) := \mathbf{\Phi}^\top(t_0 + T; \mathbf{x}_0, t_0)\mathbf{\Phi}(t_0 + T; \mathbf{x}_0, t_0) \tag{8}$$

It allows to quantify the relative stretching of nearby trajectories for a given time interval (Short, 2016). The CG tensor $\mathit{\Delta}$, symmetric and positive definite, is therefore characterized by n real positive eigenvalues: the spectral decomposition of this object enables the study of the ballistic capture process. It relates the final state offset, with respect to the initial one, by means of the following Taylor expansion:

$$\begin{aligned} ||\delta\mathbf{x}(t_0 + T)||^2 \approx \delta\mathbf{x}_0^\top \cdot \mathbf{\Phi}(\mathbf{t_0} + \mathbf{T}; \mathbf{x_0}, \mathbf{t_0})^\top \cdot \mathbf{\Phi}(\mathbf{t_0} + \mathbf{T}; \mathbf{x_0}, \mathbf{t_0}) \cdot \delta\mathbf{x}_0 = \\ = \delta\mathbf{x}_0^\top \cdot \mathit{\Delta}(T, \mathbf{x}_0, t_0) \cdot \delta\mathbf{x}_0 \end{aligned} \tag{9}$$

2.3 Implementation

In order to integrate the equations of motion and implement all the methodology outlined, making use of the SPICE ephemerides, the *GRAvity Tidal Slide* (GRATIS) toolbox has been used. Numerical integration of the equations of motion is performed, making use of the *ode113* MATLAB integrator (Shampine and Reichelt, 1997). This function makes use of an Adams-Bashforth-Moulton variable step size integration routine. Because the size of the celestial bodies are fed into GRATIS, the propagation can be stopped before any need to map the propagated state onto a singularity-free space, regularizing the equations of motion; loss of significance is nevertheless addressed in this work (Battin (2000), Section 8.4).

GRATIS works with dimensionless quantities. Physical quantities are normalized, making use of the following units: the unit of length DU is given by the mean radius of the central body. In the case of Mars, this is equal to 3396 km. The unit of time is given by $TU = \sqrt{DU^3/\mu}$, where μ is the gravitational parameter of the central body; in the case of Mars, this unit is approximately equal to 16 minutes. Finally, the spacecraft has been modelled as a point mass with a mass-to-area ratio of 40 kg/m^2, and a reflectivity of 1.1.

3 Ballistic Capture

Combining the definitions given in Belbruno (2004) and Koon et al. (2001b), ballistic capture is a phenomenon by means of which a spacecraft approaches a target celestial body and starts revolving around it only by means of interactions with two or more celestial bodies. The study of the phenomenon allows to use low-energy transfers to reach a celestial body, eliminating the need for an injection manoeuvre, and, therefore, the possibility of single-point failures.

Considering, in the context of a perturbed n-body problem, the motion of the massless particle with respect to the target body, it is possible to characterize the space of initial conditions, investigating the behaviour of the resulting trajectory. This has been done using a number of stability criteria: García and Gómez (2007) and Topputo and Belbruno (2009) introduced algorithmic categorizations for the planar case, extended by Romagnoli and Circi (2009) and Makó et al. (2010) to the 3D case; Belbruno (2004) presented analytical approximations of the same criterion. In this work, the orbit classification is performed using the method introduced in Luo et al. (2014) and expanded in Luo and Topputo (2015), in which a number of indicators, associated to the semi-plane defined by the initial conditions, are used to investigate the evolution of the trajectory. The set of initial conditions can be divided into four subsets: the n-Weakly Stable Set ($\mathcal{W}_n$), n-Unstable Set ($\mathcal{X}_n$), the n-Crash Set ($\mathcal{K}_n$) and the n-Acrobatic Set ($\mathcal{D}_n$). All the elements of the initial conditions set belong to one and only one of them.

It is relevant to notice that n can also assume negative values: backward stability is discussed in Hyeraci and Topputo (2010, 2013). This allows to define the *Capture Set*, containing all the initial conditions associated to orbits that, after being captured by the target body, naturally perform n revolutions around it:

$$\mathcal{C}_{-1}^{n} := \mathcal{X}_{-1} \cap \mathcal{W}_n \tag{10}$$

In order to rank the elements of the capture set, starting from Luo et al. (2014), a Normalized Stability Index is here used. It is given by

$$\overline{\mathcal{S}} = \frac{\mathcal{S}}{\mathcal{S}_k} \tag{11}$$

with

$$\mathcal{S} = \frac{t_n - t_0}{n}, \quad \mathcal{S}_k = 2\pi \left[\frac{r_0}{1-e_0}\right]^{3/2} \tag{12}$$

where t_n is the time at which the n^{th} revolution is completed and r_0, e_0 are the periapsis radius and the eccentricity of the initial condition: this normalization allows to investigate the stability of the orbits, irrespective of their sizes.

The Weak Stability Boundary $\partial\mathcal{W}$ can therefore be introduced: it identifies the separatrix between those points in the phase space leading to capture orbits and those leading to different behaviours, such as escape orbits. In order to identify an initial point on the WSB, a bisection method defined in polar coordinates has been here implemented, as discussed in Topputo and Belbruno (2009): the possible Cantor-like structure of the Stable Set, discussed in Sousa Silva and Terra (2012), has been here neglected. This work is focused on the identification of the closure of both the Stable Set (i.e., the Weak Stability Boundary), and of the Unstable Set.

4 Lagrangian Coherent Structures

In order to study nonlinear and non-autonomous dynamical systems, LCSs have been recently introduced[2] (Haller, 2015; Short et al., 2011; Gawlik et al., 2009; Short, 2016). The structures presented in this section are an attempt to generalize the concept of invariant manifolds, identifying transport barrier, separating regions of the phase space with qualitatively different dynamics.

4.1 Heuristics

In Gawlik et al. (2009), a particular use of Poincaré sections (Meiss, 2007) is proposed, and the Finite-Iteration Lyapunov Exponents (FILE) are introduced; with such an approach, a given hyperplane can be advected until the orbits intersect it N times.

The FILE field is related with the capture orbits categorization and, therefore, with the WSB definition: in both cases the orbit is advected for a variable time. Because of this, one could still consider the non-projected flow and introduce a

[2]While such nomenclature has been first encountered in fluid dynamics works, similar efforts had been conducted in the celestial mechanics community to investigate chaos (Froeschlé et al., 1997). Such a parallelism can be traced back to the streamline analogy given in Szebehely (1967).

time-varying Finite Time Lyapunov Exponent (FTLE)[3] field

$$\sigma_{t_0}^{T_N(\mathbf{x}_0)}(\mathbf{x}) = \frac{1}{|T_N(\mathbf{x}_0)|} \log \left\| \frac{\mathrm{d}\mathbf{\Phi}_{t_0}^{T_N(\mathbf{x}_0)}(\mathbf{x})}{\mathrm{d}\mathbf{x}} \right\| \tag{13}$$

where $T_N(\mathbf{x}_0)$, being the time it takes for the propagated orbit to intersect a section of the phase space, is a function of the initial state.

Another conceptual step away from Poincaré mapping allows to consider the intersection of the orbit in physical space with a variable 2D plane, defined by the initial condition of the orbit: in this way, each stable initial condition will be associated to a time T_N, necessary to perform N revolutions around the target body.

4.2 Time-varying Strainlines

LCSs are characterized by a number of conditions (Haller, 2010; Farazmand and Haller, 2012), one of which is given, for 2D mappings, by:

$$\xi_1(\mathbf{x}_0, t_0, T) \parallel T_{\mathbf{x}_0} \Gamma(t_0) \tag{14}$$

expressing the fact that the curve $\Gamma(t) \subset \mathbb{R}^2$, called *strainline*, is tangent to the eigenvector ξ_1, associated to the smallest eigenvalue λ_1 of the CG strain tensor $\Delta_{t_0}^{t_0+T}(\mathbf{x}_0)$. A strainline $\Gamma(t_0) \subset \mathbb{R}^2$ is obtained solving the following Cauchy problem:

$$\begin{cases} \mathbf{x}'(s) = \xi_1(\mathbf{x}(s), t_0, T) \\ \mathbf{x}(0) \ = \mathbf{x}_0 \in \Omega \\ |\xi_1| \ = 1 \end{cases} \tag{15}$$

Such strainlines lead to the definition of ridges dividing (at least in a statistical sense) the plane in dynamically distinct regions: one is therefore interested in computing the WSB, playing a similar role in ballistic capture, with a similar approach, instead of obtaining it from the computation of the capture set. In order to do this, time-varying Strainlines are introduced here.

A time-varying Strainline, $\Lambda(t) \subset \mathbb{R}^2$, is the solution of a more general Cauchy problem:

$$\begin{cases} \mathbf{x}'(s) = \xi_1(\mathbf{x}(s), t_0, T_N(s)) \\ \mathbf{x}(0) \ = \mathbf{x}_0 \in \Omega \\ |\xi_1| \ = 1 \end{cases} \tag{16}$$

where $T_N(s)$ is a function of the independent variable s through $\mathbf{x}(s)$, being the time necessary to perform N revolutions around the target body, as discussed in Section 4.1.

[3] For a discussion about the limitations of the FTLE field see, e.g., Kelley et al. (2013); Haller (2010)

4.3 Planar mapping

Because time-varying Strainlines are associated to a two-dimensional mapping, it is necessary to embed the physical flow, operating on $\mathbb{R}^6$, and introduce a new map , operating on $\mathbb{R}^2$. This procedure is synthesized in Equation (17). is related to the physical flow by means of:

$$= \pi \circ \mathcal{S} \circ \mathcal{I} \circ \phi \circ \mathcal{I}^{-1} \circ \mathcal{S}^{-1} \circ \mathcal{M} \tag{17}$$

$$\begin{Bmatrix} x_0^{OP} \\ y_0^{OP} \end{Bmatrix} \mapsto \begin{Bmatrix} x_0^{OP} \\ y_0^{OP} \\ 0 \\ \dot{x}_0^{OP} \\ \dot{y}_0^{OP} \\ 0 \end{Bmatrix} \mapsto \begin{Bmatrix} x_0^{\mathcal{S}} \\ y_0^{\mathcal{S}} \\ z_0^{\mathcal{S}} \\ \dot{x}_0^{\mathcal{S}} \\ \dot{y}_0^{\mathcal{S}} \\ \dot{z}_0^{\mathcal{S}} \end{Bmatrix} \mapsto \begin{Bmatrix} x_0 \\ y_0 \\ z_0 \\ \dot{x}_0 \\ \dot{y}_0 \\ \dot{z}_0 \end{Bmatrix} \mapsto \begin{Bmatrix} x_T \\ y_T \\ z_T \\ \dot{x}_T \\ \dot{y}_T \\ \dot{z}_T \end{Bmatrix} \mapsto \begin{Bmatrix} x_T^{\mathcal{S}} \\ y_T^{\mathcal{S}} \\ z_T^{\mathcal{S}} \\ \dot{x}_T^{\mathcal{S}} \\ \dot{y}_T^{\mathcal{S}} \\ \dot{z}_T^{\mathcal{S}} \end{Bmatrix} \mapsto \begin{Bmatrix} x_T^{OP} \\ y_T^{OP} \\ z_T^{OP} \\ \dot{x}_T^{OP} \\ \dot{y}_T^{OP} \\ \dot{z}_T^{OP} \end{Bmatrix} \mapsto \begin{Bmatrix} x_T^{OP} \\ y_T^{OP} \end{Bmatrix}$$

An initial, fixed choice of i, ω, Ω and e identifies the initial osculating Orbital Plane (OP). From there, for each given couple of values, the perigee distance r_p and its argument, it is straightforward to obtain Cartesian coordinates of any point in such place, which are used as an input for the mapping given in Eq. (17). It naturally follows that, in a three-dimensional reference frame associated to the osculating orbital parameters, the z components of the position and the velocity are both zero.

The function $\mathcal{M}$ is then introduced to compute the velocity vector, in the same reference frame, for the given value of the eccentricity. The velocity vector at perigee is given by

$$\mathbf{V_p} = V \mathbf{e_V} \tag{18}$$

with

$$V_p = \sqrt{\frac{1+e}{r_p}}, \qquad \mathbf{e_V} = [-e_{r2}, e_{r1}], \qquad \mathbf{e_r} = \frac{1}{r_p}[e_{r1}, e_{r2}]$$

The initial state of the spacecraft in the OP reference frame is hence obtained.

$\mathcal{S}$ and its inverse $\mathcal{S}^{-1}$ are reference frame transformations, relating the orbital plane with an intermediate reference frame: one may be interested in defining the initial osculating orbital plane with respect to some non-inertial reference frame (e.g., RTN@t_0), and this intermediate transformation is therefore necessary;

$\mathcal{I}$ and its inverse $\mathcal{I}^{-1}$ relate this intermediate reference frame, in which the state of the spacecraft can be computed, with the inertial reference frame, in which the equations of motion are formulated.

ϕ is the physical flow of the system and π is the projection of the final state onto the OP plane defined above; it is given by

$$\pi(x, y, z, \dot{x}, \dot{y}, \dot{z}) = (x, y) \tag{19}$$

it should be underlined that, even if the final orbital plane is different from the initial one, the Weak Stability Boundary is defined in the latter, and the Strain

Tensor should identify the direction of maximum stress in such space: this is why the projection brings the state back to the initial orbital plane.

Being the strainlines associated to ψ, and not to ϕ, the CG strain tensor is given by

$$\Delta = \Psi^\top \Psi \tag{20}$$

where Ψ is the Jacobian of ψ, computed using the chain rule:

$$\Psi = J_\psi = J_\pi J_{\mathcal{S}}^\top J_{\mathcal{I}}^\top \Phi J_{\mathcal{I}} J_{\mathcal{S}} J_{\mathcal{M}} \tag{21}$$

Φ is the State Transition Matrix of the physical flow; the Jacobian of π and $\mathcal{M}$ are given by

$$J_\pi = \begin{bmatrix} 1 & 0 & 0 & 0 & 0 & 0 \\ 0 & 1 & 0 & 0 & 0 & 0 \end{bmatrix} \qquad J_{\mathcal{M}} = \begin{bmatrix} 1 & 0 \\ 0 & 1 \\ 0 & 0 \\ \frac{\partial \dot{x}}{\partial x} & \frac{\partial \dot{x}}{\partial y} \\ \frac{\partial \dot{y}}{\partial x} & \frac{\partial \dot{y}}{\partial y} \\ 0 & 0 \end{bmatrix} \tag{22}$$

and the ones associated to rotations are straightforward. The non-trivial terms in $J_{\mathcal{M}}$ are given by:

$$\begin{aligned} \frac{\partial \dot{x}}{\partial x} &= \frac{\partial \dot{y}}{\partial y} = \sqrt{1+e}\frac{3xy}{2(x^2+y^2)^{7/4}} \\ \frac{\partial \dot{x}}{\partial y} &= \sqrt{1+e}\left(\frac{3y^2}{2(x^2+y^2)^{7/4}} - \frac{1}{(x^2+y^2)^{3/4}}\right) \\ \frac{\partial \dot{y}}{\partial x} &= \sqrt{1+e}\left(\frac{1}{(x^2+y^2)^{3/4}} - \frac{3x^2}{2(x^2+y^2)^{7/4}}\right) \end{aligned} \tag{23}$$

4.4 Methodology

The conceptual steps taken for the computation of the strainlines are the following (Figure 1):

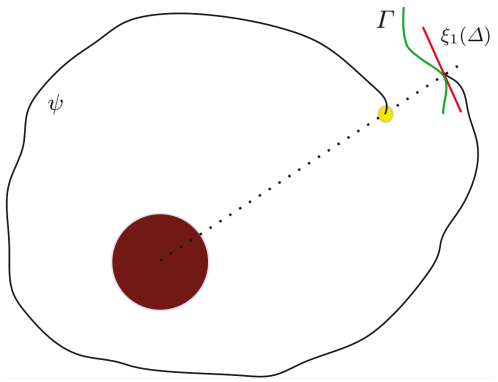

Fig. 1: Time-varying Strainlines - Conceptual Sketch

1. A bisection algorithm is applied on a 1-dimensional space, in order to find a point on the WSB;
2. the spacecraft is propagated under ϕ, until n revolutions around the target body are performed (or until the escape condition is satisfied). It should be noted that time T_1 comes from the investigation of ϕ, not ψ.
3. The variational equations are propagated until time T_1, and the Jacobian of ψ, at such epoch, is used to compute Δ.
4. The eigendecomposition of the CG strain tensor allows to identify the tangent to the strainline in the point.

These steps are used to compute the tangent to the strainline on every point: its integration solves Equation (16), leading to the Time-varying Strainline.

5 Results

We here show how the proposed technique can be use to perform ballistic capture at Mars, with an initial osculating orbit characterized by:

$$e = 0.95; \qquad \Omega = \theta = i = 0 \quad rad \tag{24}$$

Two model fidelities are considered[4], in order to test the robustness of the introduced technique. In the low-fidelity model, only the gravitational influence of Mars and of the Sun are considered, while, in the high-fidelity model, other forces are considered: the point-mass gravity of the Earth, Jupiter, Phobos and Deimos, the Solar Radiation Pressure and Mars' spherical harmonics, up to degree and order 20 (Equation (2)).

Two stable sets, associated to the low-fidelity model, are shown in Figure 2:

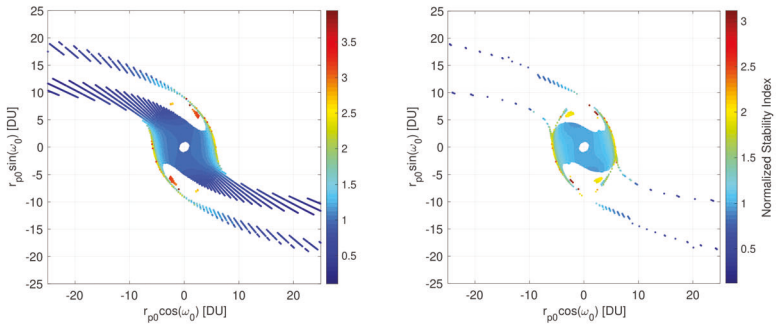

Fig. 2: Two stable sets $\mathcal{W}_1$ and $\mathcal{W}_2$, characterized by the index $\overline{\mathcal{S}}$, associated to the low-fidelity model.

[4]Design choices made here are driven by the analysis performed in Luo and Topputo (2015).

It can be noticed how the small non-connected regions of the sets are characterized, on average, by a higher Normalized Stability Index: using only the WSB to characterize a given $\mathcal{W}_n$ leads to a good approximation. This can also be appreciated in Figure 3, in which Time-varying Strainlines have been used to approximate the Stable Set.

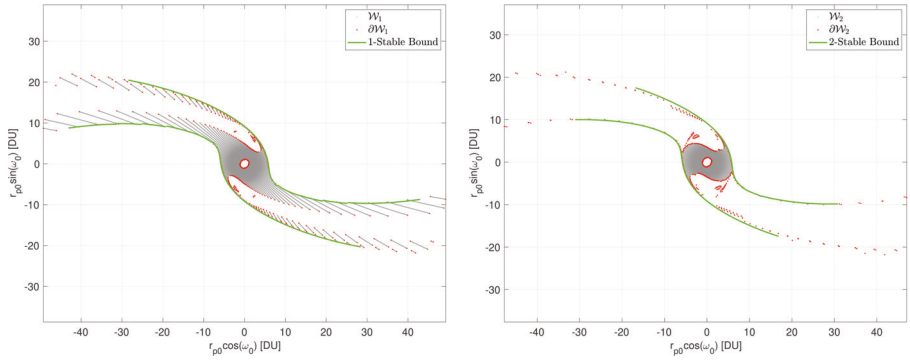

Fig. 3: Time-varying Strainlines associated to $\mathcal{W}_1$ and $\mathcal{W}_2$, in a low-fidelity model. Strainlines can be used to compute the Weak Stability Boundary.

Strainlines can also be used to characterize the motion backward in time, allowing to identify the boundary of the set $\mathcal{X}_{-1}$: the assumption (supported by the results shown in Figure 4) is that $\mathcal{K}_n \bigcup \mathcal{D}_n$ is negligible, compared to $\mathcal{X}_n \bigcup \mathcal{W}_n$. This implies that the boundary region of the two almost complementary sets is approximately the same.

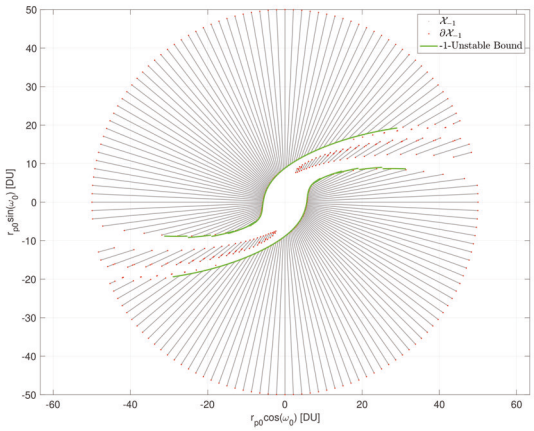

Fig. 4: Time-varying Strainlines associated to $\mathcal{X}_{-1}$, in a high-fidelity model. Strainlines can be used to characterize the motion backward in time as well.

5.1 Capture Sets and Time-varying Strainlines

The fact that a Capture Set is defined as the intersection of two other sets, $\mathcal{W}_n$ and $\mathcal{X}_{-1}$, can easily be translated, using the strainline approach, by considering the intersection of the spaces defined by them. This has been done, for the low-fidelity model, as given in Figures 5 and 6, and for the high-fidelity one, as shown in Figures 7 and 8.

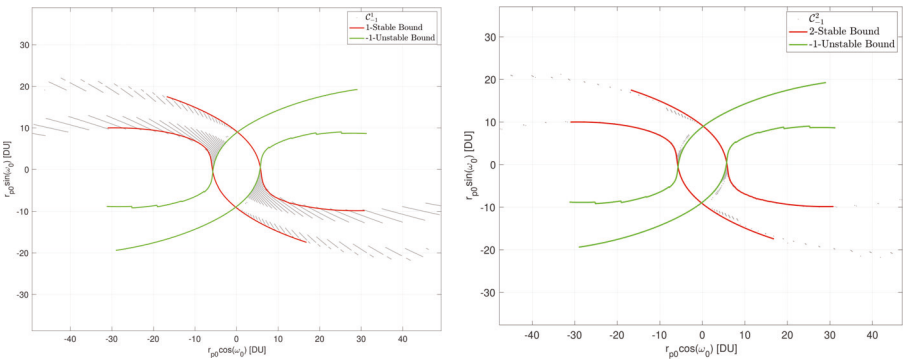

Fig. 5: Strainlines associated to $\mathcal{C}^1_{-1}$ and $\mathcal{C}^2_{-1}$ in a low-fidelity model. The intersection of the Stable and Unstable sets is represented together with the two Strainlines.

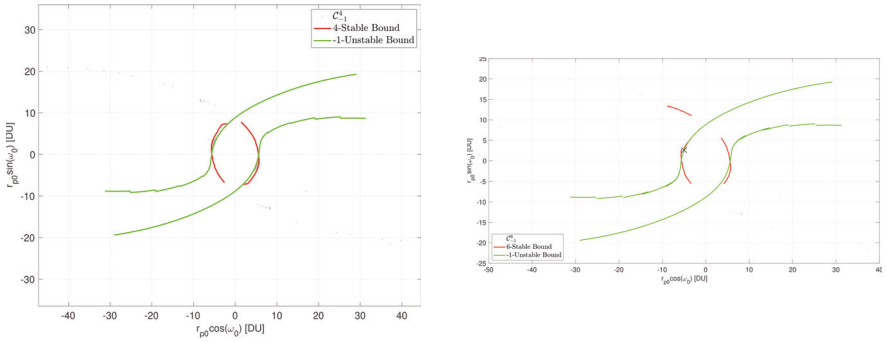

Fig. 6: Strainlines associated to $\mathcal{C}^4_{-1}$ and $\mathcal{C}^6_{-1}$ in a low-fidelity model. The intersection of the Stable and Unstable sets is represented together with the two Strainlines.

In the right plot of Figure 6, the x identifies the initial condition of the 6-Capture Set associated to the minimum normalized Stability Index. It is interesting to notice how the majority of the initial conditions leading to capture are located close

to the intersection between the stable and unstable Strainlines; this is particularly relevant for a high number of revolutions around the target.

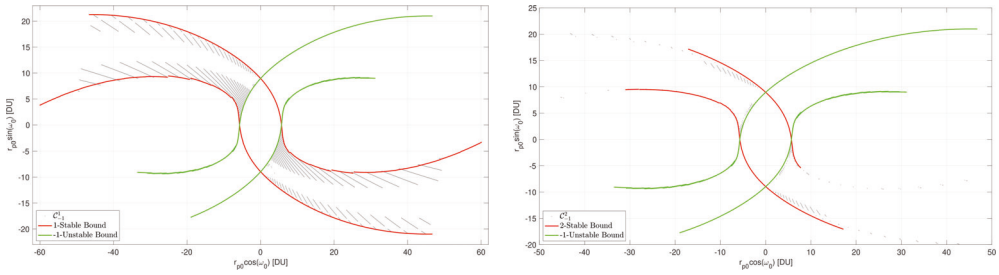

Fig. 7: Strainlines associated to $\mathcal{C}^1_{-1}$ and $\mathcal{C}^2_{-1}$ in a high-fidelity model. The flow-informed technique can be superimposed onto models of different fidelity.

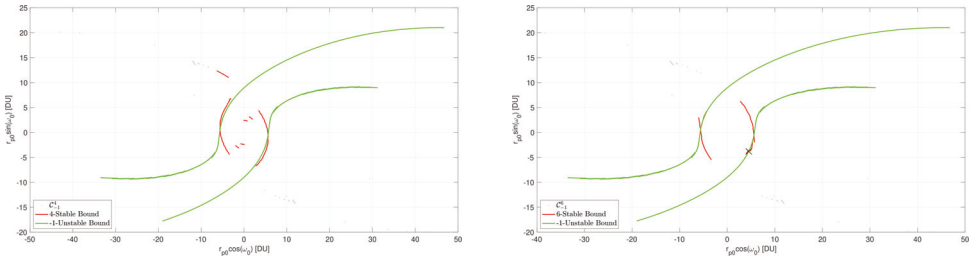

Fig. 8: Strainlines associated to $\mathcal{C}^4_{-1}$ and $\mathcal{C}^6_{-1}$ in a low-fidelity model.

5.2 Trajectories

Building from the given results, an effective routine for ballistic capture trajectory design can be proposed.

One can start computing, in the vicinity of the target body, the Time-varying Strainlines associated to the n-Stable Set of interest. From there, it's possible to restrict the computation of the Time-varying Strainline associated to $\partial\mathcal{X}_{-1}$ *inside* the stable region. From there, sampling the obtained Capture Set, particularly in the vicinity of the unstable manifold, leads to the identification of conditions associated to capture orbits.

The ΔV-free trajectories obtained with this method are shown, in different reference frames, in Figures 9 and 10. The initial conditions are the ones associated to the lowest Normalized Stability Index; they are propagated both forward and backward in time, and their stable and unstable branches can be easily identified.

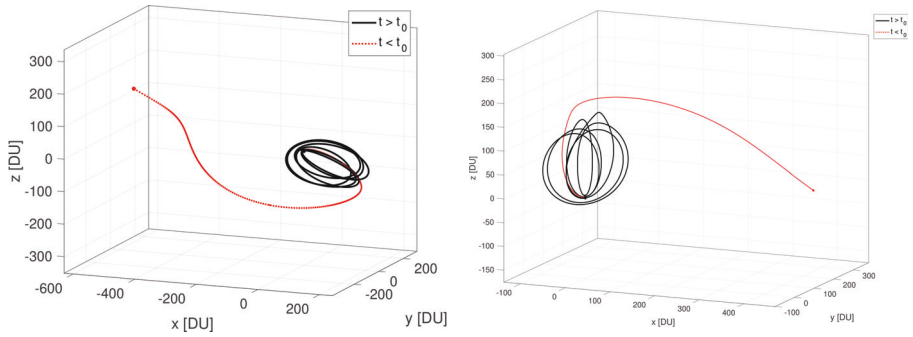

Fig. 9: Orbits, associated to the minimum Normalized Stability Index of $\mathcal{C}^6_{-1}$ for two model fidelities, in an inertial reference frame.

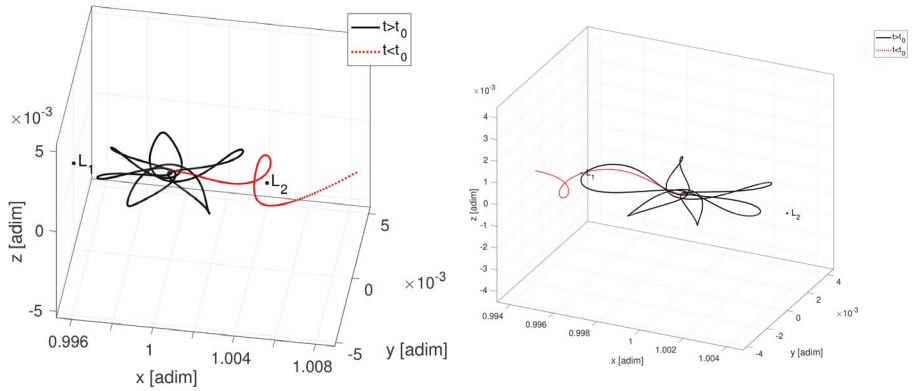

Fig. 10: Orbits, associated to the minimum Normalized Stability Index of $\mathcal{C}^6_{-1}$ for two model fidelities, in a Roto-pulsating reference frame.

6 Conclusions

The work aims at developing a ballistic capture trajectory design strategy, starting from a characterization of the phenomenon informed by the theory of Lagrangian Coherent Structures. It has been shown how the study of tools and heuristics associated to LCSs can help characterizing the mechanics of ballistic capture; with the introduction of Time-varying Strainlines, approximations of the WSBs of given problems has been computed. This has been done mainly in the domain in which the Capture Set is defined, but the flexibility of the technique allows to introduce alternative subsets of the phase space, whose investigation could lead to a clearer understanding of the ballistic capture phenomenon and of its features.

The presented results show how the effectiveness of the technique is independent of the fidelity of the underlying dynamical model, onto which the flow-informed strategy is superimposed: its applicability covers complex, non-periodic (and, in

general, time-dependent) dynamical systems in astrodynamics. Particularly for highly complex models, e.g. taking into account n-body perturbations, SRP and NSG, the technique has the potential of greatly reducing the cost of the Capture Set computation, and hence to increase the applicability of ballistic capture in trajectory design.

This work aims at contributing in opening up the field of low-energy transfers in space mission design, allowing for new concepts to redefine the domain of feasible missions for human space exploration.

A number of open questions have been identified:

the proposed technique appears to potentially reduce the cost associated to the computation of a Capture Set of interest. A quantification of the optimal trade-off between the accuracy of the WSB estimation and its efficiency, as a function of different design parameters, is missing. Moreover, the applicability of the proposed technique to different 2D subsets of the phase space should be exploited, in order to understand some features of the capture phenomenon, discussed in the literature; the same goes for generalizing the propose techniques to higher-dimensional mappings. In addition to that, alternative approaches for the computation of the Jacobian of the physical flow should be investigated, together with their accuracy and efficiency. Finally, one could aim at verifying whether Time-varying Strainlines are LCSs or not: studying whether these objects verify the other conditions may be interesting from a theoretical point of view.

Acknowledgements This work has been carried out in the context of a TU Delft Master Thesis in Space Flight.

Conflict of Interest: The authors declare that they have no conflict of interest.

References

Aguiar G., Topputo F. (2018) A technique for designing earth-mars low-thrust transfers culminating in ballistic capture. 7th International Conference on Astrodynamics Tools and Techniques

Battin R. (2000) Introduction to the Mathematics and Methods of Astrodynamics. American Institute of Aeronautics and Astronautics. Reston, VA, USA, DOI 10.2514/4.861543

Belbruno E. (2004) Capture Dynamics and Chaotic Motions in Celestial Mechanics. Princeton University Press, DOI 10.2307/j.ctv301g1f

Belbruno E., Miller J. (1993) Sun-perturbed Earth-to-Moon transfers with Ballistic Capture. Journal of Guidance, Control, and Dynamics 16, 770–775 DOI 10.2514/3.21079

Cox A., Howell K., Folta D. (2019) High-energy Lunar capture via low-thrust dynamical structures. AAS/AIAA Astrodynamics Specialist Conference, Portland, Maine (19-696)

Dei Tos D., Topputo F. (2017) Trajectory refinement of three-body orbits in the real solar system model. Advances in Space Research, 59, 2117–2132 DOI 10.1016/j.asr.2017.01.039

Farazmand M., Haller G. (2012) Computing Lagrangian Coherent Structures from their variational theory. Chaos 22, 1–12 DOI 10.1063/1.3690153

Froeschlé C., Lega E., Gonczi R. (1997) Fast lyapunov indicators. application to asteroidal motion. Celestial Mechanics and Dynamical Astronomy pp 41–62, DOI 10.1023/A:1008276418601

García F., Gómez G. (2007) A note on Weak Stability Boundaries. Celestial Mechanics and Dynamical Astronomy 97, 87-100 DOI https://doi.org/10.1007/s10569-006-9053-6

Gawlik E., Marsden J., Du Toit P., Campagnola S. (2009) Lagrangian coherent structures in the planar elliptic restricted three-body problem. Celestial Mechanics and Dynamical Astronomy 103, 227–249 DOI 10.1007/s10569-008-9180-3

Haller G. (2010) A variational theory of hyperbolic lagrangian coherent structures. Physica D 372, 31–51 DOI 10.1016/j.physd.2010.11.010

Haller G. (2015) Lagrangian coherent structures. The Annual Review of Fluid Mechanics 47, 134–161 DOI 10.1146/annurev-fluid-010313-141322

Hyeraci N., Topputo F. (2010) Method to Design Ballistic Capture in the Elliptic Restricted Three-Body Problem. Journal of Guidance, Control, and Dynamics 33, 1814–1823 DOI 10.2514/1.49263

Hyeraci N., Topputo F. (2013) The role of true anomaly in Ballistic Capture. Celestial Mechanics and Dynamical Astronomy, 116, 175–193 DOI 10.1007/s10569-013-9481-z

Jehn R., Campagnola S., Garcia D., Kemble S. (2004) Low-Thrust Approach and Gravitational Capture at Mercury. 18th International Symposium on Space Flight Dynamics (2004ESASP.548..487J)

Kelley D., Allshouse M., Ouellette N. (2013) Lagrangian coherent structures separate distinct regions in fluid flows. Physical Review, 88, 1–4 DOI 10.1103/PhysRevE.88.013017

Koon W., Lo M., Marsden J., Ross S. (2001a) Constructing a low energy tranfer between Jovian moons. Contemporary Mathematics 292, 129–146 DOI 10.1090/conm/292/04919

Koon W., Lo M., Marsden J., Ross S. (2001b) Low Energy Transfer to the Moon. Celestial Mechanics and Dynamical Astronomy 81, 63–73 DOI 10.1023/A:1013359120468

Luo Z., Topputo F. (2015) Analysis of Ballistic Capture in Sun-planet models. Advances in Space Research 56, 1030–1041 DOI 10.1016/j.asr.2015.05.042

Luo Z., Topputo F., Bernelli-Zazzera F., Tang G. (2014) Constructing Ballistic Capture orbits in the real Solar System model. Celestial Mechanics and Dynamical Astronomy 120(4), 433–450 DOI 10.1007/s10569-014-9580-5

Makó Z., Szenkovits F., Salamon J., Oláh-Gál R. (2010) Stable and unstable orbits around Mercury. Celestial Mechanics and Dynamical Astronomy, 108, 357–370 DOI 10.1007/s10569-010-9309-z

Mazanek D., Brophy J., Merrill R. (2013) Asteroid retrieval mission concept - Trailblazing our future in space and helping to protect us from Earth impactors. Planeraty Defence Conference (20130013170)

Meiss J. (2007) Differential Dynamical Systems. Society for Industrial and Applied Mathematics. Philadelphia, PA, USA, DOI 10.1137/1.9780898718232

Milani A., Gronchi G. (2004) Theory of Orbit Determination. Cambridge University Press, New York, DOI 10.1017/CBO9781139175371

Romagnoli D., Circi C. (2009) Earth-Moon Weak Stability Boundary in the restrected three- and four-body problem. Celestial Mechanics and Dynamical Astronomy 103, 79–103 DOI 10.1007/s10569-008-9169-y

Schoenmaekers J. (2004) Post-launch Optimisation of the SMART-1 Low-thrust Trajectory to the Moon. 18th International Symposium on Space Flight Dynamics (2004ESASP.548..505S)

Shampine L., Reichelt M. (1997) The MATLAB ODE Suite. SIAM Journal of Scientific Computing, 18(1), 1–22 DOI 10.1137/S1064827594276424

Short C. (2016) Flow-informed strategies for trajectory design and analysis. Purdue University, Ph.D. Dissertation

Short C., Howell K., Tricoche X. (2011) Lagrangian Coherent Structures in the Restricted Three-Body Problem. 21st AAS/AIAA Space Flight Mechanics Meeting, New Orleans, Louisiana (AAS 11-250)

Short C., Blazevsky D., Howell K., Haller G. (2015) Stretching in phase space and applications in general nonautonomous multi-body problems. Celestial Mechanics and Dynamical Astronomy 122, 213–238 DOI 10.1007/s10569-015-9617-4

Sousa Silva P., Terra M. (2012) Diversity and Validity of Stable-Unstable Transitions in the Algorithmic Weak Stability Boundary. Celestial Mechanics and Dynamical Astronomy 113, 453–478 DOI 10.1007/s10569-012-9418-y

Szebehely V. (1967) Theory of Orbits: The Restricted Problem of Three Bodies. New York: Academic Press, DOI 10.1016/B978-0-12-395732-0.X5001-6

Teramoto H., Haller G., Komatsuzaki T. (2013) Detecting invariant manifolds as stationary lagrangian coherent structures in autonomous dynamical systems. Chaos 23(4) DOI 10.1063/1.4824314

Topputo F., Belbruno E. (2009) Computation of weak stability boundaries: Sun-Jupiter system. Celestial Mechanics and Dynamical Astronomy 105, 3–17 DOI 10.1007/s10569-009-9222-5

Topputo F., Belbruno E. (2015) Earth-Mars transfers with Ballistic Capture. Celestial Mechanics and Dynamical Astronomy 121, 329–346 DOI 10.1007/s10569-015-9605-8

Wakker K. (2015) Fundamentals of Astrodynamics. Delft University of Technology, Institutional Repository, ISBN: 9789461864192